Advances in Applied Mathematics and Mechanics
Adv. Appl. Math. Mech., Vol. **18**, No. 1, pp. 242-266

DOI: 10.4208/aamm.OA-2024-0001
February 2026

The Generalized Riemann Problem for Two-Layer Shallow Water Equations with Two-Velocities

Shuzhi Liu[1] and Qinglong Zhang[2,*]

[1] *School of Statistics and Data Science, Ningbo University of Technology, Ningbo, Zhejiang 315211, China*
[2] *Corresponding author. School of Mathematics and Statistics, Ningbo University, Ningbo, Zhejiang 315211, China*

Received 4 January 2024; Accepted (in revised version) 24 May 2024

Abstract. This paper proposes a direct Eulerian generalized Riemann problem (GRP) scheme for two-layer shallow water equations. The model takes into account the distinctions between different densities and velocities, and is obtained by taking the vertical averaging across the layer depth. The source terms generated from the mass and momentum exchange prevent us from solving the Riemann problem analytically. We consider an equivalent conservative two-layer model which describes the horizontal velocity with two degrees of freedom. The rarefaction wave and the shock wave are analytically resolved by using the Riemann invariants and Rankine-Hugoniot condition, respectively. Numerical simulations are also given on some typical problems in order to verify the good performance of the GRP method.

AMS subject classifications: 35L40, 76L05, 76M12, 76B70, 65M08

Key words: Generalized Riemann problem (GRP), two-layer shallow water equations, layer-wise discretization, Riemann invariants, Rankine-Hugoniot condition.

1 Introduction

The study on the multilayer shallow water equations has been of particular interest from both theoretical and numerical points of view, mainly due to its effectively in describing the laminar shallow water models. The two layers have different densities and velocities, and can be obtained by taking the vertical averaging of the layer depth. In this work, we are interested in the following shallow water equations in one-dimensional space with

*Corresponding author.
Emails: szliu@nbut.edu.cn (S. Liu), zhangqinglong@nbu.edu.cn (Q. Zhang)

the horizontal velocity described by two variables, which reads [2]

$$\begin{cases} h_t+(h\bar{u})_x=0, \\ (h\bar{u})_t+\left(h(\bar{u}^2+\hat{u}^2)+\dfrac{g}{2}h^2\right)_x=0, \\ \hat{u}_t+(\hat{u}\bar{u})_x=0, \end{cases} \tag{1.1}$$

where $h(x,t)$ denotes the depth of the water, $\bar{u}$ and $\hat{u}$ represent the average and the oriented standard deviation of the velocities, respectively. System (1.1) introduces two degrees of velocity and was derived in [2] from a general two-layer shallow water flow. For completeness and convenience to read, we post the bilayer shallow water model with flat topography as follows [3,33]

$$\begin{cases} (h_1)_t+(h_1u_1)_x=m_e, \\ (h_1u_1)_t+\left(h_1u_1^2+g\dfrac{h_1^2}{2}+gh_1h_2\right)_x=gh_2(h_1)_x+u_{in}m_e, \\ (h_2)_t+(h_2u_2)_x=-m_e, \\ (h_2u_2)_t+\left(h_2u_2^2+g\dfrac{h_2^2}{2}\right)_x=-gh_2(h_1)_x-u_{in}m_e. \end{cases} \tag{1.2}$$

where h_i and u_i $(i=1,2)$ represent the approximation of the layer depth and the horizontal velocity of the ith layer. m_e denotes the mass exchange from the second layer to the first layer, u_{in} is the interface velocity between two layers. Actually, (1.1) can be derived from (1.2) by assuming each layer has the same depth $h_1=h_2$, and by defining

$$u_{in}=\bar{u}=\frac{u_1+u_2}{2}, \quad \hat{u}=\frac{u_2-u_1}{2}, \tag{1.3}$$

one can find more details in [2] and references therein. System (1.1) also belongs to the well-known Benney equations [10]. Other systems describing shallow water equations and related problems can be found in [21,29,30,40].

As is well known, (1.2) is conditionally hyperbolic [3,4], which bring difficulties to solve the Riemann problem. Recently, a full set of conservation laws is studied in [5,32], the local well-posedness of the two-layer shallow water equations is obtained in [31]. Numerical treatments for the two-layer shallow water equations are also available. A relaxation approach system for (1.2) is proposed and investigated by [1]. More recently, a second order central-upwind scheme was derived in [23] which is proved to be well-balanced. A novel Q-scheme is applied to the two-layer shallow water equations in [15]. More works can be found in [11,13,21,23,43] and references cited therein. Compared to the original laminar model (1.1), (1.2) has a conservative type and the source terms generated from the mass exchange and momentum exchange are cancelled out by appropriate calculations. However, (1.1) is still interesting and quite useful when we are concerned about the saturate flows. Since (1.2) is conditionally hyperbolic and the coupling between

the layers prevent the access to the system eigenstructure, the potential to design numerical schemes based on the Riemann solver is thus quite limited. In comparison, (1.1) has a quite clear eigenstructure, as one can see in [2], which allows us to apply some typical numerical treatments such as the Godunov scheme and the GRP scheme. Besides, one can generalize the method for (1.2) to other similar systems, such as the hydrostatic Navier-Stokes equations [14] and shear flows [19]. Moreover, the recover from (1.1) to (1.2) is also clear, once the state variables $(h,\bar{u},\hat{u})$ are solved numerically, one can retrieve (1.2) under the inverse transformation of (1.3).

The generalized Riemann problem (GRP) is a typical second-order method [6–9]. Basically, the GRP assumes a polynomial initial data at each time step, and a local GRP at each interface is solved in order to obtain the numerical fluxes. On the one hand, the GRP is a temporal-spatial coupling method [24] since it provides the time derivatives of the state variables near the origin. On the other hand, the GRP takes full use of the generalized Riemann invariants and Rankine-Hugoniot condition, which ensures that the method can capture both continuous and discontinuous solutions accurately. Due to its robustness, the GRP method has been widely applied in the hyperbolic systems, such as the shallow water system [25], and the radially flows [27]. Later on, a novel two-stage fourth order scheme based on the GRP method had been proposed in [26] and was used as the building block for numerical boundary conditions [20], which verified the great potential of extending the GRP method to higher order numerical schemes.

In this work, we mainly derive the GRP scheme for the laminar shallow water system (1.1). In order to obtain the second order scheme, we use the Riemann invariants to resolve the rarefaction wave under the characteristic coordinates. For the shock wave, the Rankine-Hugoniot conditions are derived and resolved along the discontinuity trajectories. Together with the two ingredients, one can obtain the cell interface fluxes by solving a pair of linear algebraic equations. The application of the GRP scheme to the shallow water equations with two velocities will enrich the research on the multilayer shallow water system. In addition, once we obtain the generalized Riemann problem for system (1.1), it is naturally to extend the GRP method to higher order numerical scheme for the original system (1.2) by using the inverse transformation of (1.3), which is forthcoming.

This paper is organized as follows. Section 2 gives some preliminaries and notations for (1.1). The characteristic form for (1.1) is also written in terms of the Riemann invariants. In Section 3, the GRP scheme for (1.1) is derived explicitly by resolving the time derivatives of the state variables at the interface. We conclude the acoustic case in Section 4, and the implementation of the GRP is outlined in Section 5. Finally, numerical simulations are presented in Section 6 to verify the effectiveness of the presented scheme.

2 Preliminaries

2.1 Characteristics form and notation

For notation convenience, we use the variables $(h,\hat{p},S)$ instead of the original variables $(h,\bar{u},\hat{u})$ to express the system, where

$$\hat{p}=\frac{g}{2}h^2+h\hat{u}^2, \quad S=\hat{u}/h. \tag{2.1}$$

As is pointed out in [2], system (2.2) is analogous to the full Euler equations at least for smooth solutions under the transformation (2.1). One can write (1.1) as follows

$$U_t+F(U)_x=0 \tag{2.2}$$

with

$$U=\begin{pmatrix} h \\ h\bar{u} \\ \hat{u} \end{pmatrix}, \quad F(U)=\begin{pmatrix} h\bar{u} \\ h(\bar{u}^2+\hat{u}^2)+\dfrac{gh^2}{2} \\ \bar{u}\hat{u} \end{pmatrix}. \tag{2.3}$$

System (2.2) has three eigenvalues, namely

$$\lambda_1=\bar{u}-c, \quad \lambda_2=\bar{u}, \quad \lambda_3=\bar{u}+c, \tag{2.4}$$

where c is the celerity given by

$$c=\sqrt{gh+3S^2h^2}. \tag{2.5}$$

The corresponding right eigenvectors are

$$\overrightarrow{r}_1=(h,-c,\hat{u})^T, \quad \overrightarrow{r}_2=\left(2h\hat{u},0,-(gh+\hat{u}^2)\right)^T, \quad \overrightarrow{r}_3=(h,c,\hat{u})^T. \tag{2.6}$$

Eq. (1.1) takes the following equivalent form for smooth flows:

$$\frac{\mathrm{D}\bar{u}}{\mathrm{D}t}+\frac{\hat{p}_x}{h}=0, \quad \frac{\mathrm{D}\hat{p}}{\mathrm{D}t}+hc^2\bar{u}_x=0, \quad \frac{\mathrm{D}S}{\mathrm{D}t}=0, \tag{2.7}$$

where $\mathrm{D}/\mathrm{D}t=\partial/\partial t+\bar{u}\partial/\partial x$ is the total derivative in the direction of the particle trajectory. In order to resolve the rarefaction wave, we look for the Riemann invariant ω_i corresponding to λ_i, which should satisfy

$$\nabla\omega_i\cdot\overrightarrow{r}_i=0, \quad i=1,3. \tag{2.8}$$

By solving (2.8), we obtain that the Riemann invariants along the λ_1 characteristic field are

$$\phi=\bar{u}-\int^h\frac{c}{h}\mathrm{d}h \quad \text{and} \quad S=\hat{u}/h, \tag{2.9}$$

the Riemann invariants along the λ_3 characteristic field are

$$\psi=\bar{u}+\int^h \frac{c}{h}\mathrm{d}h \quad \text{and} \quad S=\hat{u}/h. \tag{2.10}$$

By using the notations $\hat{p}$ and S in (2.1), the Riemann invariants can be expressed into the explicit form

$$\begin{cases} \phi=\bar{u}-\sqrt{gh+3h^2S^2}-\dfrac{g}{\sqrt{3}S}\log\left(\sqrt{1+3S^2h/g}+\sqrt{3S^2h/g}\right), \\ \psi=\bar{u}+\sqrt{gh+3h^2S^2}+\dfrac{g}{\sqrt{3}S}\log\left(\sqrt{1+3S^2h/g}+\sqrt{3S^2h/g}\right). \end{cases} \tag{2.11}$$

Furthermore, one can use the Riemann invariants ϕ and ψ to rewrite system (1.1) as the following characteristic form ([8])

$$\begin{cases} \phi_t+(\bar{u}-c)\phi_x=s_r, \\ \psi_t+(\bar{u}+c)\psi_x=s_r, \end{cases} \tag{2.12}$$

where

$$s_r=\left[\frac{gh}{S}+Sh^2-\frac{gc}{\sqrt{3}S^2}\log\left(\sqrt{1+3S^2h/g}+\sqrt{3S^2h/g}\right)\right]S_x. \tag{2.13}$$

In general, the GRP assumes piecewise polynomial initial data for the state variables, namely, we solve the GRP for (1.1) subject to the initial data

$$U(x,0)=\begin{cases} U_L+xU_L', & x<0, \\ U_R+xU_R', & x>0, \end{cases} \tag{2.14}$$

where U_L, U_R and the slope U_L' and U_R' are all constant. In order to determine the initial structure of the GRP solution $U^{GRP}(x,t)$, we need to solve the classical Riemann problem to get $U^A(x/t;U_L,U_R)$ with the initial data

$$U(x,0)=\begin{cases} U_L, & x<0, \\ U_R, & x>0, \end{cases} \tag{2.15}$$

and

$$\lim_{t\to 0+} U^{GRP}(x,t)=U^A(x/t;U_L,U_R). \tag{2.16}$$

After we obtain the classical Riemann solution, we have to obtain the time derivatives of state variables near the singularity $(x,t)=(0,0)$ by solving the generalized Riemann problem, which is the main part of the GRP scheme. The local wave solution consists of rarefaction wave, shock wave and contact discontinuity, respectively. Here we consider the wave configuration as: a rarefaction wave moves to the left and a shock wave moves to the right, with the intermediate state separated by a contact discontinuity, see Fig. 1. The intermediate states are denoted by U_1 and U_2, respectively.

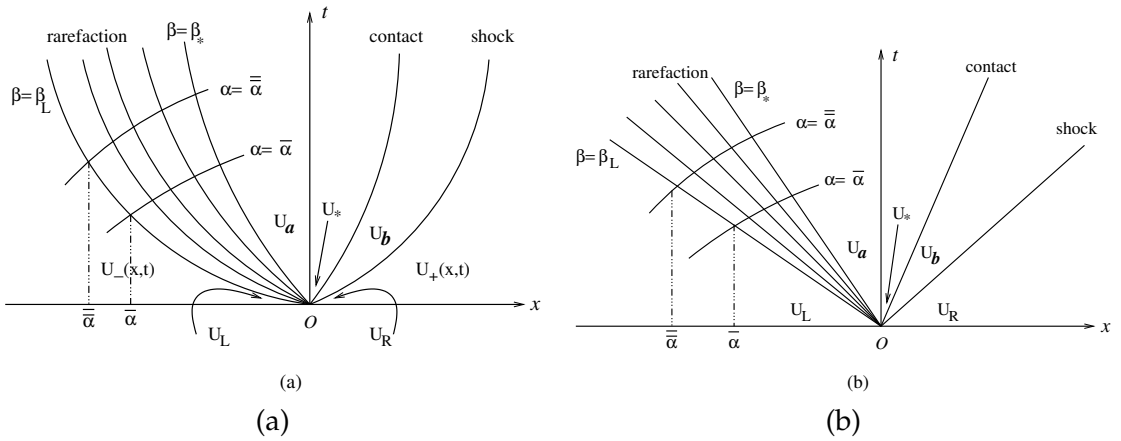

Figure 1: Typical wave patterns for the GRP (a) and the associated Riemann problem (b).

3 The generalized Riemann problem for (1.1)

In this section, we develop the GRP scheme for two-layer shallow water equations (1.1). We will resolve the rarefaction wave by using the generalized Riemann invariants under the characteristic coordinates, and resolve the shock wave by deriving the generalized Rankine-Hugoniot conditions.

3.1 Resolution of the rarefaction wave

In this subsection, we commence on resolving the rarefaction wave by using the characteristic form (2.12). To this end, we follow [9] and introduce the characteristic coordinates $\beta(x,t)$ and $\alpha(x,t)$, which are determined as follows,

$$\frac{\mathrm{d}x}{\mathrm{d}t}=\bar{u}-c,\quad \frac{\mathrm{d}x}{\mathrm{d}t}=\bar{u}+c. \tag{3.1}$$

The region of the rarefaction wave can be expressed by the set $\{(\alpha(x,t),\beta(x,t))|\beta\in[\beta_L,\beta_*],\ -\infty\leq\alpha\leq 0\}$, where α and β are denoted as follows: β is the initial slope λ_1 at the singularity $(x,t)=(0,0)$ and α is the transversal characteristic curve through the intersection point with the β_L- curve. Consequently, the coordinates (x,t) are expressed as

$$x=x(\alpha,\beta),\quad t=t(\alpha,\beta), \tag{3.2}$$

which satisfy

$$\frac{\partial x}{\partial\alpha}=\lambda_1\frac{\partial t}{\partial\alpha},\quad \frac{\partial x}{\partial\beta}=\lambda_3\frac{\partial t}{\partial\beta}. \tag{3.3}$$

Eq. (3.3) further indicates that

$$\frac{\partial}{\partial\alpha}=\frac{\partial t}{\partial\alpha}\frac{D_-}{Dt},\quad \frac{\partial}{\partial\beta}=\frac{\partial t}{\partial\beta}\frac{D_+}{Dt}, \tag{3.4}$$

where

$$\frac{D_-}{Dt}=\frac{\partial}{\partial t}+\lambda_1\frac{\partial}{\partial x},\quad \frac{D_+}{Dt}=\frac{\partial}{\partial t}+\lambda_3\frac{\partial}{\partial x}. \tag{3.5}$$

From (3.3), we differentiate the first equation with respect to β and the second equation with respect to α, which yields

$$\frac{\partial^2 t}{\partial\alpha\partial\beta}=\frac{1}{\lambda_3-\lambda_1}\left(\frac{\partial\lambda_1}{\partial\beta}\frac{\partial t}{\partial\alpha}-\frac{\partial\lambda_3}{\partial\alpha}\frac{\partial t}{\partial\beta}\right). \tag{3.6}$$

Particularly, at $\alpha=0$, we have

$$\frac{\partial\lambda_1}{\partial\beta}(0,\beta)=1,\quad \frac{\partial t}{\partial\beta}(0,\beta)=0\quad \text{for } \beta\in[\beta_L,\beta_*]. \tag{3.7}$$

Set $\alpha=0$ in (3.6), we have

$$\frac{\partial^2 t}{\partial\alpha\partial\beta}(0,\beta)=\frac{1}{\lambda_3(0,\beta)-\lambda_1(0,\beta)}\frac{\partial t}{\partial\alpha}(0,\beta), \tag{3.8}$$

which is an ordinary differential equation for the variable $(\partial t/\partial\alpha)(0,\beta)$. The key point to resolve the rarefaction wave is to obtain the values $(\mathrm{D}\bar{u}/\mathrm{D}t)_*$ and $(\mathrm{D}\hat{p}/\mathrm{D}t)_*$, which is defined by

$$\left(\frac{\mathrm{D}\bar{u}}{\mathrm{D}t}\right)_*=\frac{\mathrm{D}\bar{u}}{\mathrm{D}t}(0,\beta_*),\quad \left(\frac{\mathrm{D}\hat{p}}{\mathrm{D}t}\right)_*=\frac{\mathrm{D}\hat{p}}{\mathrm{D}t}(0,\beta_*). \tag{3.9}$$

Our main result is given in the following lemma.

Lemma 3.1. *Assume that a backward rarefaction wave moves to the left; see Fig.* 1. *The limiting values* $(\mathrm{D}\bar{u}/\mathrm{D}t)_*$ *and* $(\mathrm{D}\hat{p}/\mathrm{D}t)_*$, $\beta_L\le\beta\le\beta_*$, *satisfy the following relation:*

$$a_L\left(\frac{\mathrm{D}\bar{u}}{\mathrm{D}t}\right)_*+b_L\left(\frac{\mathrm{D}\hat{p}}{\mathrm{D}t}\right)_*=d_L, \tag{3.10}$$

where

$$(a_L,b_L)=\left(2,\frac{2}{h_*c_*}\right),\quad d_L=\frac{\mathrm{D}_-\psi}{\mathrm{D}t}(0,\beta_*)+s_r(0,\beta_*), \tag{3.11}$$

and

$$\frac{\mathrm{D}_-\psi}{\mathrm{D}t}(0,\beta_*)=\left(\frac{\mathrm{D}_-\psi}{\mathrm{D}t}\right)_L\exp\left(-\int_{\beta_L}^{\beta_*}\frac{1}{2c(0,\beta)}\mathrm{d}\beta\right)$$
$$+\exp\left(-\int_{\beta_L}^{\beta_*}\frac{1}{2c(0,\beta)}\mathrm{d}\beta\right)\int_{\beta_L}^{\beta_*}\frac{s_r(0,\tilde{\beta})}{2c(0,\tilde{\beta})}\exp\left(\int_{\beta_L}^{\tilde{\beta}}\frac{\mathrm{d}\omega}{2c(0,\omega)}\right)\mathrm{d}\tilde{\beta}, \tag{3.12}$$

with $(\partial S/\partial x)_*$ *evaluated by*

$$\left(\frac{\partial S}{\partial x}\right)_*=S_L'\frac{c_L}{c_*}\exp\left(\int_{\beta_L}^{\beta_*}-\frac{1}{c(0,\beta)}\mathrm{d}\beta\right). \tag{3.13}$$

Here $h_*=h(0,\beta_*)$, $c_*=c(0,\beta_*)$.

Proof. By using (3.4), we have

$$\frac{\partial^2\psi}{\partial\alpha\partial\beta}=\frac{\partial}{\partial\alpha}\left(\frac{\mathrm{D}_+\psi}{\mathrm{D}t}\frac{\partial t}{\partial\beta}\right)=\frac{\partial^2 t}{\partial\alpha\partial\beta}\frac{\mathrm{D}_+\psi}{\mathrm{D}t}+\frac{\partial t}{\partial\beta}\frac{\partial}{\partial\alpha}\left(\frac{\mathrm{D}_+\psi}{\mathrm{D}t}\right). \tag{3.14}$$

Similarly, from (3.4), it yields

$$\frac{\partial^2\psi}{\partial\alpha\partial\beta}=\frac{\partial}{\partial\beta}\left(\frac{\mathrm{D}_-\psi}{\mathrm{D}t}\frac{\partial t}{\partial\alpha}\right)=\frac{\partial^2 t}{\partial\alpha\partial\beta}\frac{\mathrm{D}_-\psi}{\mathrm{D}t}+\frac{\partial t}{\partial\alpha}\frac{\partial}{\partial\beta}\left(\frac{\mathrm{D}_-\psi}{\mathrm{D}t}\right). \tag{3.15}$$

Combining (3.14) and (3.15), we obtain

$$\frac{\partial^2 t}{\partial\alpha\partial\beta}\left(\frac{D_+\psi}{\mathrm{D}t}-\frac{D_-\psi}{\mathrm{D}t}\right)=\frac{\partial t}{\partial\alpha}\frac{\partial}{\partial\beta}\left(\frac{\mathrm{D}_-\psi}{\mathrm{D}t}\right)-\frac{\partial t}{\partial\beta}\frac{\partial}{\partial\alpha}\left(\frac{\mathrm{D}_+\psi}{\mathrm{D}t}\right). \tag{3.16}$$

Setting $\alpha=0$ in (3.16) and using (3.8), we get

$$\frac{1}{2c(0,\beta)}\left(s_r(0,\beta)-\frac{\mathrm{D}_-\psi}{\mathrm{D}t}(0,\beta)\right)\frac{\partial t}{\partial\alpha}(0,\beta)=\frac{\partial t}{\partial\alpha}(0,\beta)\frac{\mathrm{d}}{\mathrm{d}\beta}\left[\frac{\mathrm{D}_-\psi}{\mathrm{D}t}(0,\beta)\right], \tag{3.17}$$

which is actually an ordinary differential equation for $\frac{\mathrm{D}_-\psi}{\mathrm{D}t}(0,\beta)$ at $\alpha=0$, i.e.,

$$\frac{\mathrm{d}}{\mathrm{d}\beta}\left[\frac{\mathrm{D}_-\psi}{\mathrm{D}t}(0,\beta)\right]=-\frac{1}{2c(0,\beta)}\frac{\mathrm{D}_-\psi}{\mathrm{D}t}(0,\beta)+\frac{s_r(0,\beta)}{2c(0,\beta)},\quad \beta\in[\beta_L,\beta_*]. \tag{3.18}$$

By solving (3.18) and setting $\beta=\beta_*$, we finally obtain

$$\frac{\mathrm{D}_-\psi}{\mathrm{D}t}(0,\beta_*)=\left(\frac{\mathrm{D}_-\psi}{\mathrm{D}t}\right)_L\exp\left(-\int_{\beta_L}^{\beta_*}\frac{1}{2c(0,\beta)}\mathrm{d}\beta\right)$$
$$+\exp\left(-\int_{\beta_L}^{\beta_*}\frac{1}{2c(0,\beta)}\mathrm{d}\beta\right)\int_{\beta_L}^{\beta_*}\frac{s_r(0,\tilde{\beta})}{2c(0,\tilde{\beta})}\exp\left(\int_{\beta_L}^{\tilde{\beta}}\frac{\mathrm{d}\omega}{2c(0,\omega)}\right)\mathrm{d}\tilde{\beta}. \tag{3.19}$$

We now turn to the variation of ψ in terms of the physical variables (x,t). From (2.11) and (2.12), we have

$$\frac{\mathrm{D}_-\psi}{\mathrm{D}t}(0,\beta)=s_r(0,\beta)-2c\frac{\partial\psi}{\partial x}(0,\beta)=-\frac{2c^2}{h}\frac{\partial h}{\partial x}(0,\beta)+\frac{2}{hc}\frac{\mathrm{D}\hat{p}}{\mathrm{D}t}(0,\beta)-s_r(0,\beta), \tag{3.20}$$

where (2.7) is used. Meanwhile, from (2.1), we continue express $\partial h/\partial x$ at $(0,\beta)$

$$\frac{\partial h}{\partial x}=-\frac{h}{c^2}\frac{\mathrm{D}\bar{u}}{\mathrm{D}t}-\frac{2Sh^3}{c^2}S_x. \tag{3.21}$$

We use (3.21) to replace $\partial h/\partial x$ in (3.20) and finally have that

$$\frac{\mathrm{D}_-\psi}{\mathrm{D}t}(0,\beta)=2\frac{\mathrm{D}\bar{u}}{\mathrm{D}t}(0,\beta)+\frac{2}{hc}\frac{\mathrm{D}\hat{p}}{\mathrm{D}t}(0,\beta)-s_r(0,\beta). \tag{3.22}$$

Hence, by setting $\beta=\beta_*$ in (3.22), and combing (3.19), we derive (3.10).

For the evaluation of the value $(\partial S/\partial x)_*$, we replace ψ by S in (3.14) and (3.15), and then use (3.16) to get

$$\frac{\mathrm{d}}{\mathrm{d}\beta}(cS_x)=-S_x, \tag{3.23}$$

where $\mathrm{D}S/\mathrm{D}t=0$ is used. By integrating (3.23) and setting $\alpha=0$, $\beta=\beta_*$, we finally obtain (3.13). □

We can resolve the forward rarefaction wave in a similar way, and the explicit formulae is given in the Appendix A.

3.2 Resolution of the shock wave

In this subsection, we begin to resolve the forward shock wave as shown in Fig. 1. We will use the Rankine-Hugoniot condition to derive another relation for the values $(\mathrm{D}\bar{u}/\mathrm{D}t)_*$ and $(\mathrm{D}\hat{p}/\mathrm{D}t)_*$ along the shock trajectory.

Denote the speed of the shock wave $x=x(t)$ as $\sigma=\mathrm{d}x/\mathrm{d}t$, and the states on two sides of the shock wave as $Q(t)=Q(x(t)-0,t)$, $Q^r(t)=Q(x(t)+0,t)$. Along this shock trajectory, the Rankine-Hugoniot condition can be written in the following form,

$$\begin{cases}\sigma[h]=[h\bar{u}],\\ \sigma[h\bar{u}]=\Big[h(\bar{u}^2+\hat{u}^2)+\dfrac{g}{2}h^2\Big],\\ \sigma[\hat{u}]=[\bar{u}\hat{u}],\end{cases} \tag{3.24}$$

where "$[f]$" is the jump of the function f. By eliminating σ in (3.24) and using (2.1), (3.24) is equivalent to

$$\bar{u}=\bar{u}^r+\Phi(h;h^r,S^r), \tag{3.25}$$

where

$$\Phi(h;h^r,S^r)=(h-h^r)\sqrt{\frac{1}{hh^r}\left[(S^r)^2(h^2+hh^r+(h^r)^2)+\frac{g}{2}(h+h^r)\right]}. \tag{3.26}$$

The shock speed is

$$\sigma=\frac{h\bar{u}-h^r\bar{u}^r}{h-h^r}. \tag{3.27}$$

We take the directional derivative of (3.25) along the shock wave trajectory $x=x(t)$ and have

$$\frac{\mathrm{D}_{\text{œ}}}{\mathrm{D}t}\Gamma=0, \tag{3.28}$$

where $\mathrm{D}_\sigma/\mathrm{D}t=\partial/\partial\mathrm{t}+\sigma\partial/\partial x$, and $\Gamma=\bar{u}-\bar{u}^r-\Phi(h;h^r,S^r)$. It can be concluded that $\mathrm{D}\bar{u}/\mathrm{D}t$ and $\mathrm{D}\hat{p}/\mathrm{D}t$ are continuous in the intermediate region between the rarefaction wave and the shock wave. Thus by taking the limit $t\to 0_+$, we have

$$\frac{\mathrm{D}\bar{u}}{\mathrm{D}t}\to\left(\frac{\mathrm{D}\bar{u}}{\mathrm{D}t}\right)_*,\quad \frac{\mathrm{D}\hat{p}}{\mathrm{D}t}\to\left(\frac{\mathrm{D}\hat{p}}{\mathrm{D}t}\right)_*, \tag{3.29}$$

and

$$(h,\bar{u},\hat{p})\ \to\ (h_{2*},\bar{u}_*,\hat{p}_*),\quad (h^r,\bar{u}^r,\hat{p}^r)\ \to\ (h_R,\bar{u}_R,\hat{p}_R). \tag{3.30}$$

Note that h undergoes a jump across the contact discontinuity, we use h_{2*} to denote the limiting value of the height function between the shock wave and the contact discontinuity. The same thing would be applied to the limiting value of c_{2*}.

Lemma 3.2. *Assume that a forward shock wave moves to the right; see Fig.* 1. *The limiting values* $(\mathrm{D}\bar{u}/\mathrm{D}t)_*$ *and* $(\mathrm{D}\hat{p}/\mathrm{D}t)_*$ *satisfy the following relation:*

$$a_R\left(\frac{\mathrm{D}\bar{u}}{\mathrm{D}t}\right)_*+b_R\left(\frac{\mathrm{D}\hat{p}}{\mathrm{D}t}\right)_*=d_R, \tag{3.31}$$

where a_R, b_R *and* d_R *are given explicitly by*

$$a_R=1+\Phi_1\frac{h_{2*}(\sigma_R-\bar{u}_*)}{c_{2*}^2},\quad b_R=-\frac{\sigma_R-\bar{u}_*}{h_{2*}c_{2*}^2}-\frac{\Phi_1}{c_{2*}^2}, \tag{3.32}$$

and

$$\begin{aligned}d_R=&\left[-g-S_R^2h_R+(\sigma_R-\bar{u}_R)\Phi_2-2S_R^2h_R\right](h_R)_x+\left[\sigma_R-\bar{u}_R-h_R\Phi_2\right](\bar{u}_R)_x\\&+\left[\Phi_3(\sigma_R-\bar{u}_R)-\frac{2\Phi_1(\sigma_R-\bar{u}_*)S_Rh_{2*}^3}{c_{2*}^2}-2S_Rh_R^2\right](S_R)_x.\end{aligned} \tag{3.33}$$

Φ_1, Φ_2 and Φ_3 are defined by

$$\Phi_1=\frac{\partial\Phi}{\partial h}(h_{2*};h_R,S_R),\quad \Phi_2=\frac{\partial\Phi}{\partial h_R}(h_{2*};h_R,S_R),\quad \Phi_3=\frac{\partial\Phi}{\partial S_R}(h_{2*};h_R,S_R). \tag{3.34}$$

Proof. We follow (3.28) and take the derivative D_σ/Dt of $\Gamma=\bar{u}-\bar{u}^r-\Phi(h;h^r,S^r)$, which gives

$$\bar{u}_t+\sigma\bar{u}_x=(\bar{u}^r)_t+\sigma(\bar{u}^r)_x+\Phi_h[h_t+\sigma h_x]+\Phi_{h^r}[(h^r_t+\sigma(h^r)_x)]+\Phi_{S^r}[(S^r)_t+\sigma(S^r_x)]. \tag{3.35}$$

By using (2.7), we have

$$\bar{u}_t+\sigma\bar{u}_x=\frac{\mathrm{D}\bar{u}}{\mathrm{D}t}-\frac{\sigma-\bar{u}}{hc^2}\frac{\mathrm{D}\hat{p}}{\mathrm{D}t}, \tag{3.36}$$

where we have used the fact

$$\frac{\mathrm{D}\hat{p}}{\mathrm{D}t}=c^2\frac{\mathrm{D}h}{\mathrm{D}t} \tag{3.37}$$

from (2.1). Similarly, we have

$$h_t+\sigma h_x=\frac{\mathrm{D}h}{\mathrm{D}t}+(\sigma-\bar{u})h_x=\frac{1}{c^2}\frac{\mathrm{D}\hat{p}}{\mathrm{D}t}-\frac{h(\sigma-\bar{u})}{c^2}\frac{\mathrm{D}\bar{u}}{\mathrm{D}t}-\frac{2Sh^3}{c^2}S_x, \tag{3.38}$$

where (3.21) is applied here.

Therefore, we substitute (3.36), (3.38) into (3.35) and replace the time derivatives of h^r, $\bar{u}^r$ and S^r by their space derivatives. After that, we take the limit $t\to 0_+$ for the resulting equation to yield (3.31). □

Remark 3.1. For completeness, we also put the expressions of (3.34) directly here

$$\Phi_1=\frac{1}{\Phi(h_{2*};h_R,S_R)}\frac{h_{2*}-h_R}{2h^2_{2*}h_R}\left[3S^2_Rh^3_{2*}+S^2_R\left(h_{2*}h^2_R+h^2_{2*}h_R+h^3_R\right)+gh^2_{2*}+\frac{g}{2}h_{2*}h_R+\frac{g}{2}h^2_R\right], \tag{3.39a}$$

$$\Phi_2=-\frac{1}{\Phi(h_{2*};h_R,S_R)}\frac{h_{2*}-h_R}{2h_{2*}h^2_R}\left[3S^2_Rh^3_R+S^2_R\left(h_{2*}h^2_R+h^2_{2*}h_R+h^3_R\right)+gh^2_R+\frac{g}{2}h_{2*}h_R+\frac{g}{2}h^2_{2*}\right], \tag{3.39b}$$

$$\Phi_3=\frac{1}{\Phi(h_{2*};h_R,S_R)}\frac{h_{2*}-h_R}{h_{2*}h_R}S_R(h^3_{2*}-h^3_R), \tag{3.39c}$$

where $\Phi(h_{2*};h_R,S_R)$ is defined in (3.26).

3.3 Time derivatives of solutions at the singularity

In this section, we are ready to compute the time derivatives of $(\partial U/\partial t)_*$ in order to derive the GRP scheme. The wave structure we considered is shown in Fig. 1. Our main results are summarized in the following theorem.

Theorem 3.1 (Nonsonic case). *Assume that the t-axis is out of the rarefaction region; then the limiting values* $(\mathrm{D}\bar{u}/\mathrm{D}t)_*$ *and* $(\mathrm{D}\hat{p}/\mathrm{D}t)_*$ *are obtained by solving the following linear equations:*

$$\begin{cases} a_L\left(\dfrac{\mathrm{D}\bar{u}}{\mathrm{D}t}\right)_* + b_L\left(\dfrac{\mathrm{D}\hat{p}}{\mathrm{D}t}\right)_* = d_L, \\ a_R\left(\dfrac{\mathrm{D}\bar{u}}{\mathrm{D}t}\right)_* + b_R\left(\dfrac{\mathrm{D}\hat{p}}{\mathrm{D}t}\right)_* = d_R, \end{cases} \tag{3.40}$$

where a_L, b_L, d_L, a_R, b_R *and* d_R *are given in Lemmas* 3.1 *and* 3.2, *respectively. The coefficients of other wave configurations is given in Appendix A.*

Once we have obtained the limiting values $(\mathrm{D}\bar{u}/\mathrm{D}t)_*$ and $(\mathrm{D}\hat{p}/\mathrm{D}t)_*$, we are left to calculate the limiting values of $(\partial\bar{u}/\partial t)_*$ and $(\partial\hat{p}/\partial t)_*$. From (2.1), (2.7) and (3.21), they can be evaluated as follows

$$\left(\frac{\partial\bar{u}}{\partial t}\right)_* = -\bar{u}_*\left(\frac{\partial\bar{u}}{\partial x}\right)_* - \frac{1}{h_*}\left(\frac{\partial\hat{p}}{\partial x}\right)_* = \frac{\bar{u}_*}{h_* c_*^2}\left(\frac{\mathrm{D}\hat{p}}{\mathrm{D}t}\right)_* + \left(\frac{\mathrm{D}\bar{u}}{\mathrm{D}t}\right)_*, \tag{3.41a}$$

$$\begin{aligned}\left(\frac{\partial\hat{p}}{\partial t}\right)_* &= \left(\frac{\mathrm{D}\hat{p}}{\mathrm{D}t}\right)_* - \bar{u}_*\left(\frac{\partial\hat{p}}{\partial x}\right)_* = \left(\frac{\mathrm{D}\hat{p}}{\mathrm{D}t}\right)_* - \bar{u}_*\left[c_*^2\left(\frac{\partial h}{\partial x}\right)_* + 2S_* h_*^3 (S_x)_*\right] \\ &= \left(\frac{\mathrm{D}\hat{p}}{\mathrm{D}t}\right)_* + h_*\bar{u}_*\left(\frac{\mathrm{D}\bar{u}}{\mathrm{D}t}\right)_*.\end{aligned} \tag{3.41b}$$

When the t-axis ($x=0$) is located inside the rarefaction wave fan, then we have a sonic case; the result is given in the following theorem.

Theorem 3.2 (Sonic case). *Assume that the t-axis is in the backward rarefaction wave fan. Then we have that*

$$\left(\frac{\partial\bar{u}}{\partial t}\right)_* = \frac{1}{2}\left(\frac{\mathrm{D}_-\psi}{\mathrm{D}t}(0,\beta_*) + s_r(0,\beta_*)\right), \qquad \left(\frac{\partial\hat{p}}{\partial t}\right)_* = h_* c_* \frac{\partial\bar{u}}{\partial t}, \tag{3.42}$$

with $\beta_*=0$, *and* $\frac{\mathrm{D}_-\psi}{\mathrm{D}t}(0,\beta_*)$ *is defined in Lemma* 3.1.

Proof. On the one hand, from (2.11), we have that

$$\begin{aligned}&\frac{\mathrm{D}_-\psi}{\mathrm{D}t} = \psi_t + (u-c)\psi_x \\ =&\frac{\partial\bar{u}}{\partial t} + \frac{c}{h}\frac{\partial h}{\partial t} + \frac{c}{S}S_t - \frac{g}{\sqrt{3}S^2}\log\left(\sqrt{1+3S^2h/g}+\sqrt{3S^2h/g}\right)S_t.\end{aligned} \tag{3.43}$$

By using $\alpha=0$, $\beta_*=0$, and the fact $\mathrm{D}S/\mathrm{D}t=0$, we proceed to have that

$$\begin{aligned}&\frac{\mathrm{D}_-\psi}{\mathrm{D}t}(0,\beta_*) \\ =&\left(\frac{\partial\bar{u}}{\partial t}\right)_* + \frac{c_*}{h_*}\left(\frac{\partial h}{\partial t}\right)_* - \left[\frac{c_*^2}{S_L} - \frac{gc_*}{\sqrt{3}S_L^2}\log\left(\sqrt{1+3S_L^2h_*/g}+\sqrt{3S_L^2h_*/g}\right)\right]\left(\frac{\partial S}{\partial x}\right)_*.\end{aligned} \tag{3.44}$$

We continue to use (2.1) to replace $(\partial h/\partial t)_*$ by $(\partial \hat{p}/\partial t)_*$ and have

$$\left(\frac{\partial h}{\partial t}\right)_* = \frac{1}{c_*^2}\left(\frac{\partial \hat{p}}{\partial t}\right)_* + 2\frac{S_L h_*^3}{c_*}\left(\frac{\partial S}{\partial x}\right)_*. \tag{3.45}$$

Insert (3.45) into (3.44), we consequently have

$$\frac{\mathrm{D}_-\psi}{\mathrm{D}t}(0,\beta_*) = \left(\frac{\partial \bar{u}}{\partial t}\right)_* + \frac{1}{h_* c_*}\left(\frac{\partial \hat{p}}{\partial t}\right)_* - s_r(0,\beta_*). \tag{3.46}$$

One the other hand, in the sonic case, the t-axis is tangential to the characteristic curve at $(0,0)$, thus

$$\begin{aligned}\left(\frac{\partial \phi}{\partial t}\right)_* &= \left(\frac{\partial \phi}{\partial t}\right)_* + (u_*-c_*)\left(\frac{\partial \phi}{\partial x}\right)_* \\ &= \left(\frac{\partial \bar{u}}{\partial t}\right)_* - \frac{c_*}{h_*}\left(\frac{\partial h}{\partial t}\right)_* + \left[\frac{c_*^2}{S_L} - \frac{g c_*}{\sqrt{3}S_L^2}\log\left(\sqrt{1+3S_L^2 h_*/g}+\sqrt{3S_L^2 h_*/g}\right)\right]\left(\frac{\partial S}{\partial x}\right)_* \\ &= s_r(0,\beta_*),\end{aligned} \tag{3.47}$$

from which we have

$$\left(\frac{\partial \bar{u}}{\partial t}\right)_* - \frac{1}{h_* c_*}\left(\frac{\partial \hat{p}}{\partial t}\right)_* = 0. \tag{3.48}$$

Combining (3.44) and (3.48), we finally yield (3.42). □

Once we obtain $(\partial \bar{u}/\partial t)_*$ and $(\partial \hat{p}/\partial t)_*$, we need to compute $(\partial h/\partial t)_*$. It depends on whether the contact discontinuity propagates to the left or the right. The result is given in the following theorem.

Theorem 3.3 (The computation of $(\partial h/\partial t)_*$)**.**

(i) If $\bar{u}_* > 0$, we compute the value $(\partial h/\partial t)_*$ on the left side

$$\left(\frac{\partial h}{\partial t}\right)_* = \frac{1}{c_*^2}\left(\frac{\partial \hat{p}}{\partial t}\right)_* + 2\frac{S_L h_*^3 \bar{u}_*}{c_*^2}\left(\frac{\partial S}{\partial x}\right)_*. \tag{3.49}$$

(ii) If $\bar{u}_* < 0$, we compute the value $(\partial h/\partial t)_*$ on the right side

$$\left(\frac{\partial h}{\partial t}\right)_* = \frac{h_* \bar{u}_*}{c_*^2}\left(\frac{\mathrm{D}\bar{u}}{\mathrm{D}t}\right)_* + \frac{1}{c_*^2}\left(\frac{\mathrm{D}\hat{p}}{\mathrm{D}t}\right)_* + \frac{2S_R h_*^3 \bar{u}_*}{c_*^2}\frac{\sigma_R - \bar{u}_R}{\sigma_R - \bar{u}_*}S_R'. \tag{3.50}$$

Proof. For the first case that $\bar{u}_* > 0$, it can be derived directly from (2.1). For the second case $\bar{u}_* < 0$, we first take the directional derivative with $\hat{p}$ and have that

$$\left(\frac{\mathrm{D}\hat{p}}{\mathrm{D}t}\right)_* + (\sigma-\bar{u}_*)\left(\frac{\partial \hat{p}}{\partial x}\right)_* = c_*^2\left[\left(\frac{\mathrm{D}h}{\mathrm{D}t}\right)_* + (\sigma-\bar{u}_*)\left(\frac{\partial h}{\partial x}\right)_*\right] + 2S_R h_*^3(\sigma-\bar{u}_R)S_R'. \tag{3.51}$$

From (2.7), we substitute $(\hat{p}_x)_*=-h_*(\mathrm{D}\bar{u}/\mathrm{D}t)_*$ into (3.51) and have that

$$\left(\frac{\partial h}{\partial x}\right)_*=-\frac{h_*}{c_*^2}\left(\frac{\mathrm{D}\bar{u}}{\mathrm{D}t}\right)_*-\frac{2s_Rh_*^3}{c_*^2}\frac{\sigma_R-\bar{u}_R}{\sigma_R-\bar{u}_*}S_R'. \tag{3.52}$$

Finally, from the fact that

$$\left(\frac{\mathrm{D}h}{\mathrm{D}t}\right)_*=\frac{1}{c_*^2}\left(\frac{\mathrm{D}\hat{p}}{\mathrm{D}t}\right)_*,$$

we have (3.50). □

4 Acoustic case

Acoustic case appears when $U_L=U_R$ and $U_L'\neq U_R'$. In this case, only linear waves emanate from the origin. The GRP scheme is simple which is stated in the following theorem.

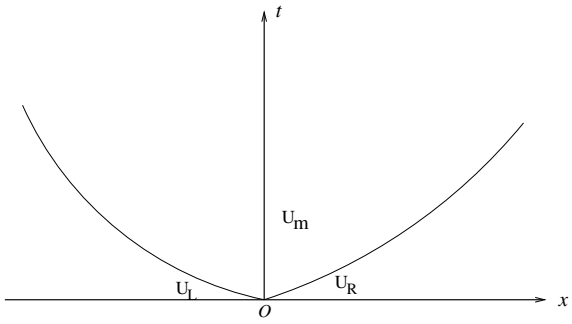

Figure 2: The schematic description for the GRP scheme in acoustic case.

Theorem 4.1 (Acoustic case). *For the acoustic case, if $u_*-c_*<0$ and $u_*+c_*>0$, then $(\partial\bar{u}/\partial t)_*$ and $(\partial\hat{p}/\partial t)_*$ is given by*

$$\left(\frac{\partial\bar{u}}{\partial t}\right)_*=\frac{\bar{u}_*-c_*}{2}\left(\frac{\hat{p}_R'}{c_*h_R}-\bar{u}_R'\right)-\frac{\bar{u}_*+c_*}{2}\left(\frac{\hat{p}_L'}{c_*h_L}+u_L'\right), \tag{4.1a}$$

$$\left(\frac{\partial\hat{p}}{\partial t}\right)_*=\frac{h_*(\bar{u}_*-c_*)}{2}\left(-\frac{\hat{p}_R'}{h_R}+c_*\bar{u}_R'\right)-\frac{h_*(\bar{u}_*+c_*)}{2}\left(\frac{\hat{p}_L'}{h_L}+c_*u_L'\right). \tag{4.1b}$$

The computation of $(\partial h/\partial t)_*$ is given by

$$\left(\frac{\partial h}{\partial t}\right)_*=\begin{cases}\dfrac{1}{c_*^2}\left(\dfrac{\partial\hat{p}}{\partial t}\right)_*+2\dfrac{S_Lh_*^3\bar{u}_*}{c_*^2}S_L', & \text{if } \bar{u}_L=\bar{u}_R=\bar{u}_*>0,\\ \dfrac{1}{c_*^2}\left(\dfrac{\partial\hat{p}}{\partial t}\right)_*+2\dfrac{S_Rh_*^3\bar{u}_*}{c_*^2}S_R', & \text{if } \bar{u}_L=\bar{u}_R=\bar{u}_*<0.\end{cases} \tag{4.2}$$

Proof. Denote the intermediate state $U_m(x,t)$ which is separated by $U_-(x,t)$ and $U_+(x,t)$. First, we differentiate $\bar{u}$ along characteristic curve $u-c$ and have that

$$\frac{\partial \bar{u}_-}{\partial t}+(\bar{u}-c)\frac{\partial \bar{u}_-}{\partial x}=\frac{\partial \bar{u}_m}{\partial t}+(\bar{u}-c)\frac{\partial \bar{u}_m}{\partial x}, \tag{4.3}$$

which gives

$$\frac{\mathrm{D}\bar{u}_-}{\mathrm{D}t}-c\frac{\partial \bar{u}_-}{\partial x}=\frac{\mathrm{D}\bar{u}_m}{\mathrm{D}t}+\frac{1}{hc}\frac{\mathrm{D}\hat{p}_m}{\mathrm{D}t} \tag{4.4}$$

by using (2.7). Thus, by taking the limit $t\to 0_+$, we have

$$\left(\frac{\mathrm{D}\bar{u}_m}{\mathrm{D}t}\right)_*+\frac{1}{h_*c_*}\left(\frac{\mathrm{D}\hat{p}_m}{\mathrm{D}t}\right)_*=-\frac{\hat{p}'_L}{h_L}-c_*u'_L. \tag{4.5}$$

Similarly, consider the acoustic wave moving to the right, we have

$$\frac{\partial \bar{u}_+}{\partial t}+(\bar{u}+c)\frac{\partial \bar{u}_+}{\partial x}=\frac{\partial \bar{u}_m}{\partial t}+(\bar{u}+c)\frac{\partial \bar{u}_m}{\partial x}, \tag{4.6}$$

which leads to

$$\left(\frac{\mathrm{D}\bar{u}_m}{\mathrm{D}t}\right)_*-\frac{1}{h_*c_*}\left(\frac{\mathrm{D}\hat{p}_m}{\mathrm{D}t}\right)_*=-\frac{\hat{p}'_R}{h_R}+c_*u'_R. \tag{4.7}$$

From (4.5) and (4.7), we obtain that

$$\begin{cases} \left(\dfrac{\mathrm{D}\bar{u}_m}{\mathrm{D}t}\right)_*=\dfrac{1}{2}\left[-\dfrac{\hat{p}'_L}{h_L}-\dfrac{\hat{p}'_R}{h_R}+c_*\left(u'_R-u'_L\right)\right], \\ \left(\dfrac{\mathrm{D}\hat{p}_m}{\mathrm{D}t}\right)_*=\dfrac{h_*c_*}{2}\left[-\dfrac{\hat{p}'_L}{h_L}+\dfrac{\hat{p}'_R}{h_R}-c_*\left(u'_R+u'_L\right)\right]. \end{cases} \tag{4.8}$$

Substitute (4.8) into (3.41), we finally get (4.1).

The computation of $(\partial h/\partial t)_*$ can be obtained by taking the partial derivative with respect to t of $\hat{p}$ in (2.1), which yields (4.2). □

5 Implementation of the GRP scheme

We will summarize the main steps to implement the GRP scheme for (1.1). Assume that the grid points are equally discretized with $x_j=j\Delta x, j\in\mathbb{Z}$, the interface is denoted as $x_{j+1/2}=(x_j+x_{j+1})/2$. Denote U_j^n as the averaged value of U over the cell $I_j=[x_{j-1/2},x_{j+1/2}]$ at $t_n=n\Delta t$. The GRP scheme is implemented through the following four steps.

Step I. Given the piecewise polynomial initial data

$$U^n(x)=U_j^n+\sigma_j^n(x-x_j),\quad x\in(x_{j-1/2},x_{j+1/2}), \tag{5.1}$$

where σ_j^n is the initial slope over cell I_j. We solve the classical Riemann problem to get $U_{j+1/2}^n$

$$U_{j+1/2}^n = R\left(0 : U_j^n + \frac{\Delta x}{2}\sigma_j^n, U_{j+1}^n - \frac{\Delta x}{2}\sigma_{j+1}^n\right). \tag{5.2}$$

Step II. Compute the time derivative $(\partial U/\partial t)_{j+1/2}^n$ from a linear equations as in Theorem 3.1. One can find more details in [9]. The mid-point values $U_{j+1/2}^{n+1/2}$ can be approximated by

$$U_{j+1/2}^{n+1/2} = U_{j+1/2}^n + \frac{\Delta t}{2}\left(\frac{\partial U}{\partial t}\right)_{j+1/2}^n. \tag{5.3}$$

Step III. Update the values U_j^{n+1} at the next time step by

$$U_j^{n+1} = U_j^n - \frac{\Delta t}{\Delta x}\left(F(U_{j+1/2}^{n+1/2}) - F(U_{j-1/2}^{n+1/2})\right). \tag{5.4}$$

Step IV. Finally, update the slope as follows,

$$U_{j+1/2}^{n+1,-} = U_{j+1/2}^n + \Delta t\left(\frac{\partial U}{\partial t}\right)_{j+1/2}^n, \tag{5.5a}$$

$$\sigma_j^{n+1,-} = \frac{1}{\Delta x}(U_{j+1/2}^{n+1,-} - U_{j-1/2}^{n+1,-}). \tag{5.5b}$$

Here a minmod limiter is used,

$$\sigma_j^{n+1} = \text{minmod}\left(\alpha\frac{U_j^{n+1} - U_{j-1}^{n+1}}{\Delta x}, \sigma_j^{n+1,-}, \alpha\frac{U_{j+1}^{n+1} - U_j^{n+1}}{\Delta x}\right), \tag{5.6}$$

where the parameter $\alpha \in [0,2)$. For more details, we refer to [6].

Remark 5.1. We can check that the GRP scheme satisfies the well-balancing property, i.e., it can keep the exact solution to the lake-at-rest problem [12]. Consider the flat bottom, and assume that $\bar{u}_j^n = 0$, $\hat{u}_j^n = 0$, $h_j^n \equiv const.$, then from (5.6), we have $\sigma_j^n = 0$. With the results obtained in Section 3, we get

$$\left(\frac{\partial h}{\partial t}\right)_{j+1/2}^n = 0, \quad \left(\frac{\partial \bar{u}}{\partial t}\right)_{j+1/2}^n = 0, \quad \left(\frac{\partial \hat{u}}{\partial t}\right)_{j+1/2}^n = 0. \tag{5.7}$$

Thus, from (5.3), we have

$$h_{j+1/2}^{n+1/2} = h_{j+1/2}^n, \quad (h\bar{u})_{j+1/2}^{n+1/2} = (h\bar{u})_{j+1/2}^n = 0, \quad \hat{u}_{j+1/2}^{n+1/2} = \hat{u}_{j+1/2}^n = 0. \tag{5.8}$$

Therefore,

$$h_j^{n+1}=h_j^n-\frac{\Delta t}{\Delta x}\left((h\bar{u})_{j+1/2}^{n+1/2}-(h\bar{u})_{j-1/2}^{n+1/2}\right)=h_j^n, \tag{5.9}$$

and

$$(h\bar{u})_j^{n+1}=(h\bar{u})_j^n-\frac{\Delta t}{\Delta x}\left(\left(h\bar{u}^2+h\hat{u}^2+\frac{1}{2}gh^2\right)_{j+1/2}^{n+1/2}-\left(h\bar{u}^2+h\hat{u}^2+\frac{1}{2}gh^2\right)_{j-1/2}^{n+1/2}\right)=0, \tag{5.10a}$$

$$\hat{u}_j^{n+1}=\hat{u}_j^n-\frac{\Delta t}{\Delta x}\left((\hat{u}\bar{u})_{j+1/2}^{n+1/2}-(\hat{u}\bar{u})_{j-1/2}^{n+1/2}\right)=\hat{u}_j^n. \tag{5.10b}$$

This implies that $h_j^{n+1}=h_j^n$, $\bar{u}_j^{n+1}=\bar{u}_j^n$, $\hat{u}_j^{n+1}=\hat{u}_j^n$. Thus, we proved the well-balancing property of the scheme. We note that the well-balancing property can also be extended to the non-flat bottom topography, see [25] for more details. It is also very important to consider other kinds of well-balancing properties for a numerical scheme, such as preserving all the equilibria, or reconstruct the wet-dry front [17,18,36–39,41,42], which will be discussed later for the GRP scheme.

Remark 5.2. The GRP scheme can also be generalized to hyperbolic system with source terms and multidimensional fluid dynamics. Recently, the GRP solver is taken as a representative of L-W type schemes for the construction of a two-stage fourth order scheme [26], which shows a great potential to extend the GRP scheme to higher order numerical methods.

6 Numerical tests

In this section, we present some numerical simulations to verify the expected accuracy and effectiveness of the GRP scheme for (1.1). In the following examples, we take $g=9.81$ and CFL $=0.5$ unless specified.

Example 6.1 (Smooth initial value problem)**.** This example is used to verify the order of accuracy of the GRP method. Similar with [23,36], we take the initial data as

$$h(x,0)=5+e^{\sin(2\pi x)},\quad u_1(x,0)=\sin(\cos(2\pi x)),\quad u_2(x,0)=\sin(\cos(2\pi x))+1.0, \tag{6.1}$$

with $0\leq x\leq 1.0$. Periodic boundary conditions are used on both sides. We compute the solution up to $t=0.1$ and the CFL = 0.1 in order to reach the expected order. The numerical solutions are compared with the reference solution computed with 10000 cells. The L_1 errors and L_∞ errors of the height function $h(x,t)$ are shown in Table 1, from which one can observe the convergence of second order is almost reached.

Example 6.2 (Interface propagation)**.** This example is taken from [1] with a slight modification. The goal is to test the ability of the method capturing interface propagation. The

Table 1: The L_1, L_∞ errors of the height and numerical order of the GRP for the smooth initial value problem in Example 6.1.

Number of zones	L_1 error	Order	L_∞ error	Order
25	1.127e-1	–	2.573e-1	–
50	3.591e-2	1.65	8.667e-2	1.57
100	1.193e-2	1.59	3.001e-2	1.53
200	3.402e-3	1.81	8.860e-3	1.76
400	8.928e-4	1.93	2.458e-3	1.85

initial data is set as

$$(h(x,0),u_1(x,0),u_2(x,0))=\begin{cases}(2.56,2.5,4.5), & 0\le x\le 50,\\ (3.25,0.871,3.409), & 50<x\le 100.\end{cases} \tag{6.2}$$

The solution involves a hydraulic jump which is initially located at $x=50$. The output time is $t=2.0$. The results are computed by using 100 meshes, see Fig. 3. One can find that the GRP solution captures the hydraulic jump sharply with few grids.

Example 6.3 (Riemann problem)**.** We test the typical Riemann problem in this case for (1.1). The initial data is set as

$$(h(x,0),u_1(x,0),u_2(x,0))=\begin{cases}(4.0,0.25,1.25), & 0\le x\le 50,\\ (1.0,1.0,3.0), & 50<x\le 100.\end{cases} \tag{6.3}$$

The output time is $t=3.0$. The Riemann solution involves a backward rarefaction wave, followed by a contact discontinuity and a forward shock wave. We use 200 meshes (100 grids are shown), and compare the results obtained by the GRP method with the second-order central-upwind method [22, 23] in Fig. 4, which indicates that the GRP method gives a sharp resolution for both smooth wave and also discontinuity solutions.

Example 6.4 (Large water height ratio problem)**.** The large water height ratio problem is modified from the large pressure ratio problem in [35], which is used to test the ability of the scheme to capture the location of strong rarefaction. Here we apply this example to the two-layer shallow water equations (1.1). The initial data is set as

$$(h(x,0),u_1(x,0),u_2(x,0))=\begin{cases}(50.0,1.5,5.0), & 0\le x\le 50,\\ (1.0,0.5,1.5), & 50<x\le 100,\end{cases} \tag{6.4}$$

in order to produce a high water jump initially. The boundary condition is dealt the same with that in the standard Riemann problem. The output time is $t=3.0$. We test the example with 150 meshes (left) and 400 meshes (right). respectively. In Fig. 5, compared to the central-upwind solution, the GRP solution resolve the strong rarefaction wave and the shock wave quite well with small number of grids.

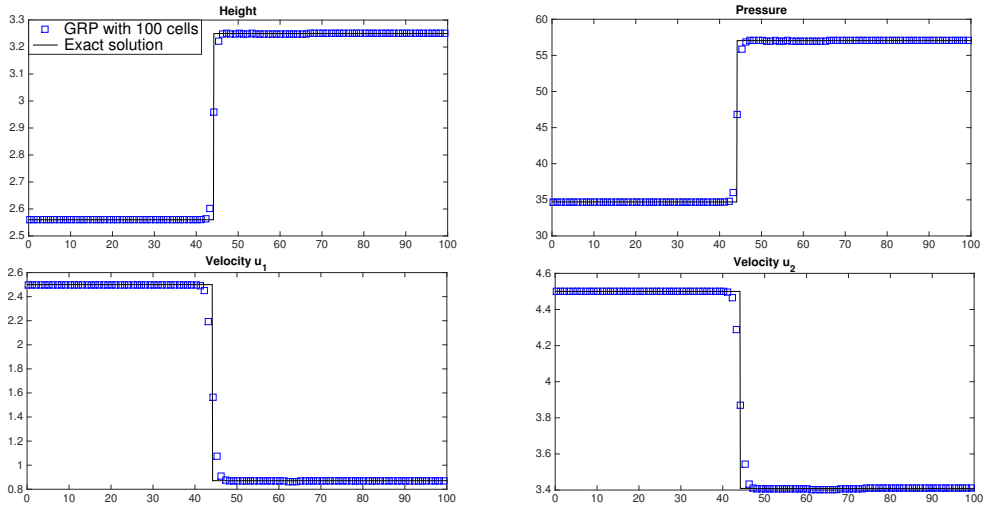

Figure 3: The hydraulic jump in Example 6.2.

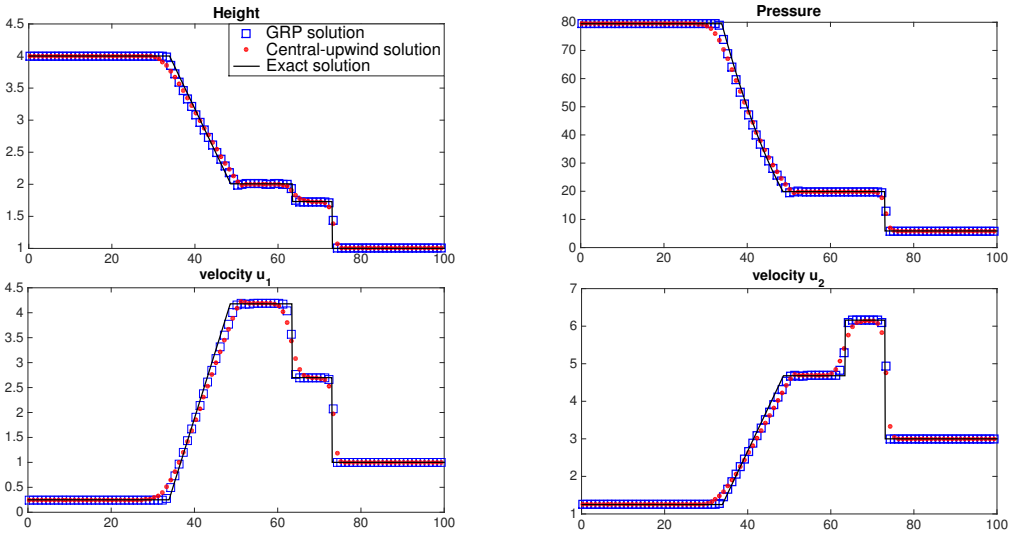

Figure 4: Comparison of the Riemann solution obtained by the GRP solver with that obtained by the central-upwind method in Example 6.3.

Example 6.5 (Periodic boundary problem)**.** In this example, we aim to test model (1.1) with periodic numerical conditions. The initial data is given by

$$(h(x,0),u_1(x,0),u_2(x,0))=(1.0,\sin(0.3\pi x)+2.0,\sin(0.3\pi x)+1.0). \tag{6.5}$$

The periodic boundary conditions are used here. A very challenging problem is to capture both the water peaks and valleys during the waves propagation. Both smooth solutions and discontinuous solutions are tested here. In the first case, the output time is

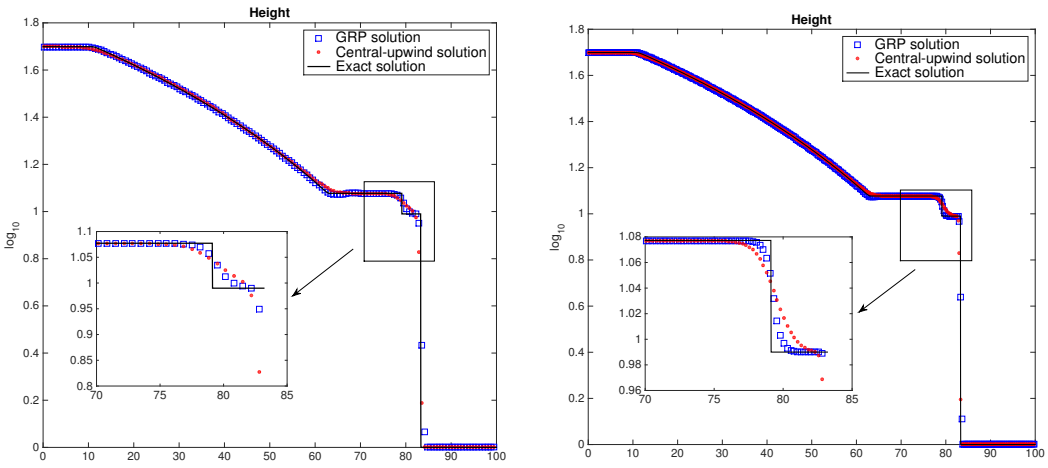

Figure 5: Comparison of numerical results of the water depth h obtained by the GRP scheme and the central-upwind scheme with 150 meshes (left) and 400 meshes (right).

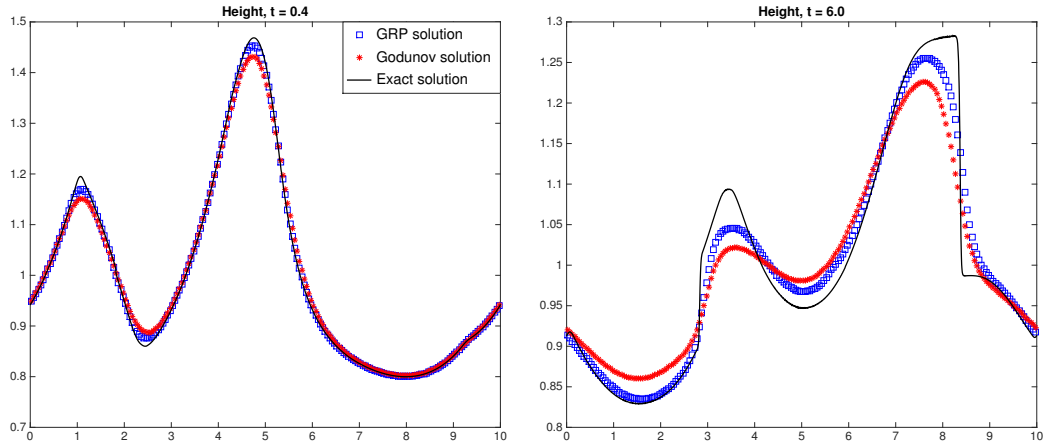

Figure 6: Numerical results for water waves problem in Example 6.5.

$t=0.4$, the smooth GRP solution is tested with 200 meshes, see Fig. 6(left). The solution then develops a shock wave at the output time $t=6.0$, see Fig. 6(right). We compare the numerical results with the reference solution, which is obtained by using 2000 grids. In both cases, the GRP scheme shows stable results and matches well with the amplitude variations of the reference solution from peaks to valleys.

Example 6.6 (Moving boundary problem)**.** The moving boundary problem is used to test the scheme's ability to capture complex reflected wave structures. It is the one-dimensional version from [16], see also in [34]. Initially, there is a rigid body located at $x=50$ traveling with constant speed $v=1.0$, the two-layer water depth and velocities

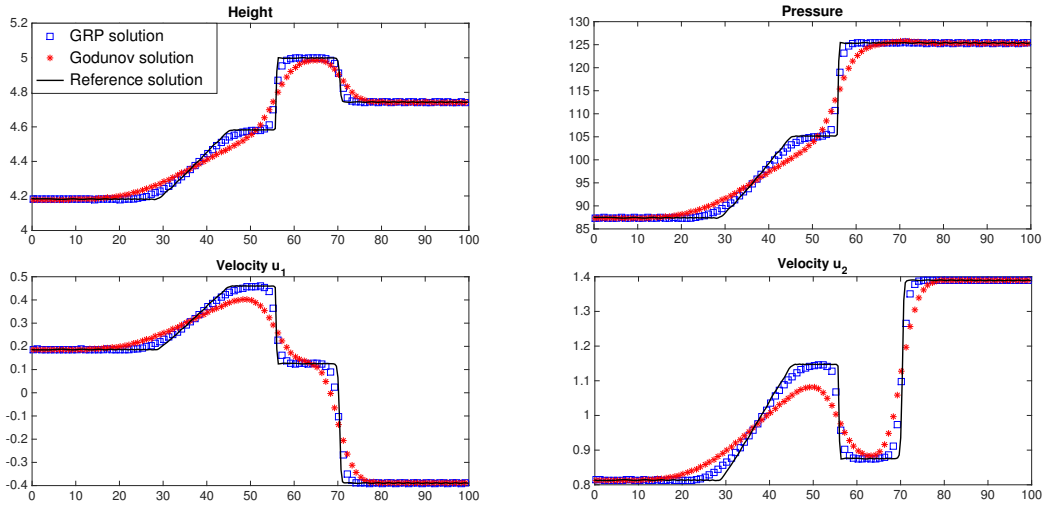

Figure 7: Numerical results for moving boundary problem in Example 6.6.

are given by

$$(h(x,0),u_1(x,0),u_2(x,0))=\begin{cases}(5.0,0.25,1.75), & 0\leq x\leq 50,\\ (4.0,-0.5,2.5), & 50<x\leq 100.\end{cases} \tag{6.6}$$

When the water interacts with the rigid body, the following reflected boundary conditions is imposed

$$h^n_{M+1}=h^n_M,\quad (u_1)^n_{M+1}=2.0-(u_1)^n_M,\quad (u_2)^n_{M+1}=2.0-(u_2)^n_M, \tag{6.7}$$

where the cell M is on the right hand side of the boundary. By implementing the GRP scheme on the problem with the output time $t=13.5$, we compare the GRP solutions with the Godunov solution in Fig. 7, from which one can obviously observe that the GRP has potential in capturing the complex reflected waves.

7 Discussions

This paper proposes and implements a generalized Riemann problem (GRP) for two-layer shallow water equations with two velocities. By resolving the Riemann invariants associated with the two-layer model and the Rankine-Hugoniot conditions, we determine the time derivatives of the state variables which is the main theme of the scheme. Numerical simulations are also presented to validate the performance of the GRP. Of course, some issues remain for the future study, such as the applications of the GRP in the framework of two-stage fourth order time stepping [26], and also use the GRP as the building block for the numerical treatment of boundary conditions [20, 28].

Appendix

A The useful GRP coefficients

The coefficients of the GRP scheme are collected here. In Table 2, the 1-shock (3-shock, resp.) refers to the forward shock corresponding with the $\bar{u}-c$ characteristic family ($\bar{u}+c$, resp.). The same for the 1-rarefaction wave and 3-rarefaction wave.

Table 2: The coefficients in Theorem 3.1 for all possible cases.

1-rarefaction wave	$(a_L,b_L)=(a_L^{\text{rare}},b_L^{\text{rare}}),d_L=d_L^{\text{rare}}$
1-shock wave	$(a_L,b_L)=(a_L^{\text{shock}},b_L^{\text{shock}}),d_L=d_L^{\text{shock}}$
3-rarefaction wave	$(a_R,b_R)=(a_R^{\text{rare}},b_R^{\text{rare}}),d_R=d_R^{\text{rare}}$
3-shock wave	$(a_R,b_R)=(a_R^{\text{shock}},b_R^{\text{shock}}),d_R=d_R^{\text{shock}}$

A.1 Nonsonic case

The coefficients for rarefaction waves are given by

$$(a_L^{\text{rare}},b_L^{\text{rare}})=\left(2,\frac{2}{h_{1*}c_{1*}}\right),\qquad (a_R^{\text{rare}},b_R^{\text{rare}})=\left(2,-\frac{2}{h_{2*}c_{2*}}\right),\tag{A.1a}$$

$$d_L^{\text{rare}}=\frac{\mathrm{D}_-\psi}{\mathrm{D}t}(0,\beta_*)+s_r(0,\beta_*),\qquad d_R^{\text{rare}}=\frac{\mathrm{D}_+\phi}{\mathrm{D}t}(\alpha_*,0)+s_r(\alpha_*,0),\tag{A.1b}$$

where $\mathrm{D}_-\psi/\mathrm{D}t(0,\beta_*)$ is given in Lemma 3.1, and $\mathrm{D}_+\phi/\mathrm{D}t(\alpha_*,0)$ is denoted by

$$\begin{aligned}\frac{\mathrm{D}_+\phi}{\mathrm{D}t}(\alpha_*,0)=&\left(\frac{\mathrm{D}_+\phi}{\mathrm{D}t}\right)_R\exp\left(\int_{\alpha_*}^{\alpha_R}\frac{1}{2c(\alpha,0)}\mathrm{d}\alpha\right)\\&+\exp\left(\int_{\alpha_*}^{\alpha_R}\frac{1}{2c(\alpha,0)}\mathrm{d}\alpha\right)\int_{\alpha_*}^{\alpha_R}\frac{-s_r(\tilde{\alpha},0)}{2c(\tilde{\alpha},0)}\exp\left(\int_{\alpha_*}^{\tilde{\alpha}}\frac{-\mathrm{d}\omega}{2c(0,\omega)}\right)\mathrm{d}\tilde{\alpha},\end{aligned}\tag{A.2}$$

with $(\partial S/\partial x)_{2*}$ evaluated by

$$\left(\frac{\partial S}{\partial x}\right)_{2*}=S_R'\frac{c_R}{c_{2*}}\exp\left(\int_{\alpha_*}^{\alpha_R}\frac{1}{c(\alpha,0)}\mathrm{d}\alpha\right).\tag{A.3}$$

The coefficients for shocks are given by

$$a_L=1-\Phi_1(h_{1*};h_L,S_L)\frac{h_{1*}(\sigma_L-\bar{u}_{1*})}{c_{1*}^2},\qquad b_L=-\frac{\sigma_L-\bar{u}_*}{h_{1*}c_{1*}^2}+\frac{\Phi_1(h_{1*};h_L,S_L)}{c_{1*}^2},\tag{A.4a}$$

$$d_L=\left[g+S_L^2h_L+(\sigma_L-\bar{u}_L)\Phi_2(h_{1*};h_L,S_L)+2S_L^2h_L\right](h_L)_x-\left[\sigma_L-\bar{u}_L+h_L\Phi_2(h_{1*};h_L,S_L)\right](\bar{u}_L)_x$$
$$+\left[\Phi_3(h_{1*};h_L,S_L)(\sigma_L-\bar{u}_L)+\frac{2\Phi_1(h_{1*};h_L,S_L)(\sigma_L-\bar{u}_*)S_Lh_{1*}^3}{c_{1*}^2}+2S_Lh_L^2\right](S_L)_x, \quad \text{(A.4b)}$$

$$a_R=1+\Phi_1(h_{2*};h_R,S_R)\frac{h_{2*}(\sigma_R-\bar{u}_*)}{c_{2*}^2}, \qquad b_R=-\frac{\sigma_R-\bar{u}_*}{h_{2*}c_{2*}^2}-\frac{\Phi_1(h_{2*};h_R,S_R)}{c_{2*}^2}, \quad \text{(A.4c)}$$

$$d_R=\left[-g-S_R^2h_R+(\sigma_R-\bar{u}_R)\Phi_2(h_{2*};h_R,S_R)-2S_R^2h_R\right](h_R)_x$$
$$+\left[\sigma_R-\bar{u}_R-h_R\Phi_2(h_{2*};h_R,S_R)\right](\bar{u}_R)_x+\Big[\Phi_3(h_{2*};h_R,S_R)(\sigma_R-\bar{u}_R)$$
$$-\frac{2\Phi_1(h_{2*};h_R,S_R)(h_{2*};h_R,S_R)(\sigma_R-\bar{u}_*)S_Rh_{2*}^3}{c_{2*}^2}-2S_Rh_R^2\Big](S_R)_x, \quad \text{(A.4d)}$$

where

$$\Phi_1(h;\hat{h},\hat{S})=\frac{1}{\Phi(h;\hat{h},\hat{S})}\frac{h-\hat{h}}{2h^2\hat{h}}\left[3\hat{S}^2h^3+\hat{S}^2\left(h\hat{h}^2+h^2\hat{h}+\hat{h}^3\right)+gh^2+\frac{g}{2}h\hat{h}+\frac{g}{2}\hat{h}^2\right], \quad \text{(A.5a)}$$

$$\Phi_2(h;\hat{h},\hat{S})=-\frac{1}{\Phi(h;\hat{h},\hat{S})}\frac{h-\hat{h}}{2h\hat{h}^2}\left[3\hat{S}^2\hat{h}^3+\hat{S}^2\left(h\hat{h}^2+h^2\hat{h}+\hat{h}^3\right)+g\hat{h}^2+\frac{g}{2}h\hat{h}+\frac{g}{2}h^2\right], \quad \text{(A.5b)}$$

$$\Phi_3(h;\hat{h},\hat{S})=\frac{1}{\Phi(h;\hat{h},\hat{S})}\frac{h-\hat{h}}{h\hat{h}}\hat{S}(h^3-\hat{h}^3), \quad \text{(A.5c)}$$

and $\Phi(h;\hat{h},\hat{S})$ is defined in (3.26).

A.2 Sonic case

When the t-axis is located inside the right rarefaction fan, we have

$$\left(\frac{\partial\bar{u}}{\partial t}\right)_*=\frac{1}{2}\left(\frac{\mathrm{D}_+\phi}{\mathrm{D}t}(\alpha_*,0)+s_r(\alpha_*,0)\right), \qquad \left(\frac{\partial\hat{p}}{\partial t}\right)_*=-h_*c_*\frac{\partial\bar{u}}{\partial t}, \quad \text{(A.6)}$$

where $\alpha_*=0$, and $\frac{\mathrm{D}_+\phi}{\mathrm{D}t}(\alpha_*,0)$ is defined in Lemma (A.2).

Acknowledgements

This work is supported by NSFC (Nos. 12201329, 12201323 and 12272059), and Zhejiang Provincial Natural Science Foundation of China (No. LQ22A010001). The authors are very grateful to the anonymous referees for their corrections and suggestions, which improved the original manuscript greatly.

References

[1] R. ABGRALL, AND S. KARNI, *Two-layer shallow water systems: A relaxation approach*, SIAM J. Sci. Comput., 31 (2009), pp. 1603–1627.

[2] N. AGUILLON, E. AUDUSSE, E. GODLEWSKI, AND M. PARISOT, *Analysis of the Riemann problem for a shallow water model with two velocities*, SIAM J. Math. Anal., 5 (2018), pp. 4861–4888.
[3] E. AUDUSSE, *A multilayer Saint-Venant model: Derivation and numerical validation*, Discrete Contin. Dyn. Syst. Ser. B, 5 (2005), pp. 189–214.
[4] E. AUDUSSE, M. BRISTEAU, B. PERTHAME, AND J. SAINTE-MARIE, *A multilayer Saint-Venant system with mass exchanges for shallow water flows. Derivation and numerical validation*, ESAIM: Math. Model. Numer. Anal., 45 (2011), pp. 169–200.
[5] B. BARROS, *Conservation laws for one-dimensional shallow water models for one and two-layer flows*, Math. Models Methods Appl. Sci., 16 (2006), pp. 119–137.
[6] M. BEN-ARTZI, AND J. FALCOVITZ, *A second-order Godunov-type scheme for compressible fluid dynamics*, J. Comput. Phys., 55 (1984), pp. 1–32.
[7] M. BEN-ARTZI, AND J. FALCOVITZ, Generalized Riemann Problems in Computational Fluid Dynamics, Cambridge University Press, 2003.
[8] M. BEN-ARTZI, AND J. LI, *Hyperbolic balance laws: Riemann invariants and the generalized Riemann problem*, Numer. Math., 106 (2007), pp. 369–425.
[9] M. BEN-ARTZI, J. LI, AND G. WARNECKE, *A direct Eulerian GRP scheme for compressible fluid flows*, J. Comput. Phys., 218 (2006), pp. 19–43.
[10] D. J. BENNEY, *Some properties of long nonlinear waves*, Stud. Appl. Math., 52 (1973), pp. 45–50.
[11] F. BERGER, AND J. F. COLOMBEAU, *Numerical solutions of one-pressure models in multifluid flows*, SIAM J. Numer. Anal., 32 (1995), pp. 1139–1154.
[12] A. BOLLERMANN, G, CHEN, A. KURGANOV, AND S. NOELLE, *A well-balanced reconstruction of wet/dry fronts for the shallow water equations*, J. Sci. Comput., 56 (2013), pp. 267–290.
[13] F. BOUCHUT, AND T. MORALES DE LUNA, *An entropy satisfying scheme for two-layer shallow water equations with uncoupled treatment*, M2AN Math. Model. Numer. Anal., 42 (2008), pp. 683–698.
[14] M. O. BRISTEAU, B. DI-MARTINO, C. GUICHARD, AND J. SAINTE-MARIE, *Layer-averaged Euler and Navier-Stokes equations*, Commun. Math. Sci., 15 (2017), pp. 1221–1246.
[15] M. CASTRO, J. MACIÁS, AND C. PARÉS, *A Q-scheme for a class of system of coupled conservation laws with source term. Application to a two-layer 1-D shallow water system*, M2AN Math. Model. Numer. Anal., 35 (2001), pp. 107–127.
[16] D. M. CAUSON, D. M. INGRAM, AND C. G. MINGHAN, *A Cartesian cut cell method for shallow water flows with moving boundaries*, Adv. Water Res., 24 (2001), pp. 899–911.
[17] G. CHEN, AND S. NOELLE, *A unified surface-gradient and hydrostatic reconstruction scheme for the shallow water equations*, J. Comput. Phys., 467 (2022), 111463.
[18] G. CHEN, AND S. NOELLE, *A new hydrostatic reconstruction scheme based on subcell reconstructions*, SIAM J. Numer. Anal., 55 (2017), pp. 758–784.
[19] A. CHIAPOLINO, AND R. SAUREL, *Models and methods for two-layer shallow water flows*, J. Comput. Phys., 371 (2018), pp. 1043–1066.
[20] Z. DU, AND J. LI, *A two-stage fourth order time-accurate discretization for Lax-Wendroff type flow solvers II. High order numerical boundary conditions*, J. Comput. Phys., 369 (2018), pp. 125–147.
[21] S. GAVRILYUK, K. IVANOVA, AND N. FAVRIE, *Multi-dimensional shear shallow water flows: Problems and solutions*, J. Comput. Phys., 366 (2018), pp. 252–280.
[22] A. KURGANOV, S. NOELLE, AND G. PETROVA, *Semi-discrete central-upwind scheme for hyperbolic conservation laws and Hamilton-Jacobi equations,* SIAM J. Sci. Comput., 23 (2001), pp. 707–740.
[23] A. KURGANOV, AND G. PETROVA, *Central-upwind schemes for two-layer shallow water equa-*

tions, SIAM J. Sci. Comput., 31 (2009), pp. 1742–1773.
[24] J. LI, *Two-stage fourth order: Temporal-spatial coupling in computational fluid dynamics (CFD)*, Adv. Aerodynam., 1 (2019), pp. 1–36.
[25] J. LI, AND G. CHEN, *The generalized Riemann problem method for the shallow water equations with bottom topography*, Int. J. Numer. Methods Eng., 65 (2006), pp. 834–862.
[26] J. LI, AND Z. DU, *A two-stage fourth order temporal discretization for on the Lax-Wendroff type flow solvers* I. *Hyperbolic conservation laws*, SIAM, J. Sci. Comput., 38 (2016), pp. 3046–3069.
[27] J. LI, T. LIU, AND Z. SUN, *Implementation of the GRP scheme for computing radially symmetric compressible fluid flows*, J. Comput. Phys., 228 (2009), pp. 5867–5887.
[28] J. LI, AND Q. ZHANG, *One-sided GRP solver and numerical boundary conditions for compressible fluid flows*, J. Comput. Phys., 459 (2022), 111138.
[29] S. LIU, AND Q. ZHANG, *Axisymmetric solutions of the shallow water equations with bottom topography*, Res. Math. Sci., 9 (2022), pp. 1–17.
[30] R. R. LONG, *Long waves in a two-fluid system*, J. Met., 13 (1956), pp. 70–74.
[31] R. MONJARRET, *Local well-posedness of the two-layer shallow water model with free surface*, SIAM J. Appl. Math., 75 (2015), pp. 2311–2332.
[32] P. J. MONTGOMERY, AND T. G. MOODIE, *On the number of conserved quantities for the two-layer shallow water equations*, Stud. Appl. Math., 106 (2001), pp. 229–259.
[33] L. OVSYANNIKOV, *Two-layer "shallow water" model*, J. Appl. Mech. Tech. Phys., 20 (1979), pp. 127–135.
[34] L. QIAN, D. M. CAUSON, C. G. MINGHAM, AND D. M. INGRAM, *A free-surface capturing method for two fluid flows with moving bodies*, Proc. R. Soc. A, 462 (2006), pp. 21–42.
[35] H. Z. TANG, AND T. G. LIU, *A note on the conservative schemes for the Euler equations*, J. Comput. Phys., 218 (2006), pp. 451–459.
[36] X. WANG, AND G. CHEN, *A Positivity-preserving well-balanced wet-dry front reconstruction for shallow water equations on rectangular grids*, Appl. Numer. Math., 198 (2024), pp. 295–317.
[37] R. YAN, W. TONG, AND G. CHEN, *A well-balanced positivity-preserving multidimensional central scheme for shallow water equations*, Appl. Numer. Math., 197 (2024), pp. 97–118.
[38] R. YAN, W. TONG, AND G. CHEN, *A mass conservative, well balanced and positivity-preserving central scheme for shallow water equations*, Appl. Math. Comput., 443 (2023), 127778.
[39] R. YAN, W. TONG, AND G. CHEN, *An efficient invariant-region-preserving central scheme for hyperbolic conservation laws*, Appl. Math. Comput., 436 (2023), 127500.
[40] Q. ZHANG, W. SHENG, AND Y. ZHENG, *Interaction of the elementary waves for shallow water equations with discontinuous topography*, Commun. Math. Sci., 19 (2021), pp. 1381–1402.
[41] J. ZHANG, Y. XIA, AND Y. XU, *Structure-preserving finite volume arbitrary Lagrangian-Eulerian WENO schemes for the shallow water equations*, J. Comput. Phys., 473 (2023), 111758.
[42] W. ZHANG, Y. XIA, AND Y. XU, *Positivity-preserving well-balanced arbitrary Lagrangian-Eulerian discontinuous Galerkin methods for the shallow water equations*, J. Sci. Comput., 88 (2021), pp. 1–43.
[43] F. ZHAO, J. GAN, AND K. XU, *High-order compact gas-kinetic scheme for two-layer shallow water equations on unstructured mesh*, J. Comput. Phys., 498 (2024), 112651.